International Conference on Space Optics—ICSO 2014

La Caleta, Tenerife, Canary Islands

7–10 October 2014

Edited by Zoran Sodnik, Bruno Cugny, and Nikos Karafolas

The CarbonSat candidate mission: radiometric and spectral performances over spatially heterogeneous scenes

J. Caron

B. Sierk

J.-L. Bezy

A. Loescher

et al.

esa icso proceedings cnes

International Conference on Space Optics — ICSO 2014, edited by Zoran Sodnik, Nikos Karafolas, Bruno Cugny, Proc. of SPIE Vol. 10563, 105633J · © 2014 ESA and CNES
CCC code: 0277-786X/17/$18 · doi: 10.1117/12.2304186

THE CARBONSAT CANDIDATE MISSION: RADIOMETRIC AND SPECTRAL PERFORMANCES OVER SPATIALLY HETEROGENEOUS SCENES

J. Caron[1], B. Sierk[2], J.L. Bezy[2], A. Loescher[2], Y. Meijer[1]
[1]*ESA-Estec, co RHEA system BV, The Netherlands.* [2]*ESA-Estec, The Netherlands.*

CarbonSat is one of the two candidate missions for the 8th cycle of European Space Agency (ESA) Earth Explorers, currently undergoing feasibility studies with two industrial consortia. The mission aims at quantifying the spatial distribution of carbon dioxide (CO_2) and methane (CH_4) with high precision (3.0 ppm for CO_2 and 12.0 ppb for CH_4) and accuracy (0.5 ppm for CO_2 and 5 ppb for CH_4) at a high spatial resolution (2km x 3km) and with global coverage above 40° latitude every 12 days. It consists of three pushbroom spectrometers measuring the Earth reflectance in each of the following bands: NIR (747nm-773nm @0.1nm resolution), SWIR-1 (1590-1675nm @0.3nm) and SWIR-2 (1925-2095nm @0.55nm).

Although most requirements for the CarbonSat phase A are defined over spatially homogeneous scenes, it is known from previous missions and studies that the observation of real, spatially heterogeneous scenes create specific measurement errors. One obvious mechanism is a distortion of the instrument spectral response function (ISRF) induced by a non-uniform slit illumination in the along-track (ALT) direction. This error has been analysed for several missions (OMI, Sentinel-4, Sentinel-5). The combination of spectrometer smile with across-track (ACT) scene non-uniformities induces similar errors. In this paper, we report about the analysis efforts carried out during CarbonSat preliminary phases to evaluate and mitigate these effects. In a first section, we introduce common concepts and notations for heterogeneous scenes analysis. An exhaustive list of known error mechanisms is presented. In section 2 we discuss the effect of inhomogeneous slit illumination, and describe hardware mitigation with a slit homogeniser. The combination of spectrometer smile and ACT heterogeneities is studied in section 3.

I. COMMON CONCEPTS AND NOTATIONS FOR HETEROGENEOUS SCENE ANALYSIS

A. Parametrization of heterogeneous scenes

Spatial heterogeneities may be induced by variations in the atmospheric layers (clouds, aerosol layers, ground altitude) and/or variations of ground albedo. As the foreseen CO_2 and CH_4 retrievals are only possible in cloud-free conditions, and atmospheric scattering plays a lesser role in the CarbonSat SWIR bands it is natural to focus on ground albedo variations. A convenient parametrisation that has been traditionally used at ESA consists in a linear interpolation between two spectra, corresponding to the same atmospheric state but obtained with dark and bright albedos, and an interpolation weight w(x,y) carrying all spatial dependencies:

$$\mathrm{L}(\lambda, x, y) = \left[1 - w(x, y)\right] \mathrm{L}_{dark}(\lambda) + w(x, y)\, \mathrm{L}_{bright}(\lambda) \tag{1}$$

If w(x,y) remains within the interval [0,1] the interpolation may be also interpreted as a weighted superposition. This parametrisation is practical as the spatial and spectral dependencies are well separated. The instrument PSFs will only impact the weights w(x,y) in (1) when the signal propagates through the instrument. For the purpose of the analyses required in phases A/B1 of CarbonSat, two types of heterogeneous scenes have been considered as shown on Fig.1: (a) uni-dimensional "contrast scenes", where the weight varies only along the x (ALT) or y (ACT) direction and takes only two values, 0 or 1 (b) realistic scenes, where the weights have the full 2D variability and can take any value. These scenes aim at representing real cases and the weights are computed from MODIS reflectance (resolution 500m) or AVIRIS radiance (typ. resolution 5m-20m) data.

B. Known error mechanisms and their assessment

An exhaustive list of error mechanisms occuring over heterogeneous scenes is presented in table 1. Column 5 describes the behavior of each error wrt temporal averaging. While the satellite is flying, spatial heterogeneities create fast temporal fluctuations in the measured signal. As the overlap between consecutive spatial samples is limited, and becomes negligible between samples N and N+2, the associated correlation length is very short. For most errors, the temporal average reduces quickly to zero but in a few case a systematic error component is created. Column 6 indicates the possibility to describe an error spectrally. "Spectral" errors have a spectral average equal to zero : they consist in a spectral re-distribution of the detected photons and can be described with ISRF distortion. For "radiometric" errors photons are added or subtracted to the useful signal.

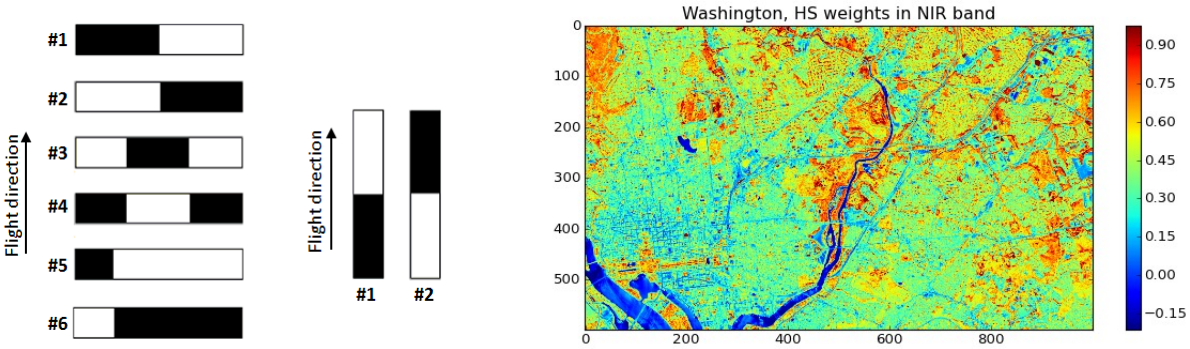

Fig. 1. Contrast scenes in ACT and ALT directions (left), real scene computed from AVIRIS data over Washington area (right) obtained on 6 July 2009, 1000*600 pixels with sampling 16.8m.

Effect name	**Description**	**ALT/ ACT**	**Mitigation**	**Residual after averaging**	**Error type**
Non-uniform slit filling	The slit illumination is not uniform and creates a distorted ISRF	ALT	Software (correction with temporally oversampled data [1,2,3]) or hardware (slit homogeniser)	No	Spectral
Spectrometer smile + ACT HS	Spectral calibration is variable in ACT across a spatial sample. Non-uniform illumination shifts the ISRF.	ACT	Smile-free spectrometer design, stable detector positionning	No	Spectral
PRNU + ACT binning + ACT HS	Different pixels see different levels of signals. PRNU correction is performed after binning	ACT	PRNU correction before binning	No	Radiometric
NL + ACT binning or temporal co-addition	Different pixels or temporal measurements see different levels of signals. NL correction is performed after binning (ACT) or co-addition (temporal).	ALT+ ACT	NL correction before binning	Systematic component	Radiometric
Memory effect	Measurement N carries a fraction of measurement N-1	ALT	Linear part of memory effect is not critical, equivalent to ALT mis-registration. Non-linear effect usually small	Systematic component	Radiometric
Mis-registration	Error comes from spectral variations of the instrument footprint.	ALT+ ACT	Specific requirements (intra-band/inter-band co-registration for footprint centroid)	No	Radiometric

Tab. 1. List of error mechanisms over heterogeneous scenes.

To evaluate the impact of these mechanisms, the most natural way would be to compute a dot product between a gain vector and the reflectance error spectrum, mapping directly the error on level-2 products. Then, part of the mission requirements for CarbonSat on rms (precision) and systematic (accuracy) level-2 errors for CO_2 and CH_4 may be allocated to each error in table 1. Unfortunately, the error-free measured signal and therefore the gain vector depend on the part of the scene that is actually measured (instrument position and footprint). In these conditions, a parametrisation or interpolation of the gain vector between L_{dark} and L_{bright} seems to be the only practical way to assess level-2 errors without a full retrieval algorithm. Preliminary

attempts to derive such parametrisation indicate that a high sampling between L_{dark} and L_{bright} is required. Further efforts are on-going in this direction. For the spectral errors, an alternative possibility is to link the resulting ISRF distortion to scientific requirements on ISRF shape and centroid position knowledges. Such ISRF requirements applicable over contrast scenes in ALT and ACT have been used during the phases A-B1 of Sentinel-5 and CarbonSat, and are investigated in the next sections.

II. IMPACT OF ALONG-TRACK SCENE HETEROGENEITIES

A. Problem overview

The most obvious effect of scene heterogeneities comes from the non-uniform slit illumination, and consists in a deformation of the ISRF. Its impact on measurements was discovered in-flight during the OMI mission, and could be corrected thanks to the availability of temporally oversampled data [1]. The errors resulting from non-uniform illumination of the slit in the ALT direction have been studied for many missions, including Sentinel-4, Sentinel-5 and CarbonSat [2-5]. Besides software correction [2,3], hardware mitigation is possible with slit homogeniser devices, and has been considered for Sentinel-5 and CarbonSat [4,6].

The measurement error can be modelled as follows. The scene radiance given by (1) is re-written assuming heterogeneities in along-track only

$$\mathrm{L}\left(\lambda_0, x\right) = \mathrm{L}_0\left(\lambda_0\right) + w\left(x\right)\Delta\mathrm{L}\left(\lambda_0\right) \tag{2}$$

We propagate this radiance through the instrument: blurring with the smear and telescope optics, cutting by the slit edges, blurring again by the spectrometer and detector PSF, and conversion of x into a spectral coordinate:

$$\begin{aligned} &\mathrm{L}_{measured}\left(\lambda_0, \lambda\right) = \left[\mathrm{L}_0\left(\lambda_0\right) + \tilde{w}\left(x\right)\Delta\mathrm{L}\left(\lambda_0\right)\right] Slit\left(x\right) \otimes \underset{detector}{PSF_{spectro+}}\left(x, y\right) \otimes k\delta\left[x - k\left(\lambda - \lambda_0\right)\right] \\ &\tilde{w}\left(x\right) = w\left(x\right) \otimes \underset{telescope}{PSF_{smear+}}\left(x, y\right) \end{aligned} \tag{3}$$

k is a linear dispersion coefficient (spatial units per spectral units); it is also needed in front of the Dirac function for normalisation. Two spectral coordinates are used: λ_0, wavelength of the monochromatic incident light, and λ, spectral coordinate of the measurement. To evaluate the radiometric error, this measured radiance can be compared to its error-free radiometric equivalent obtained by replacing the blurred weight with its average across the slit width:

$$W = \int \tilde{w}\left(x\right) Slit\left(x\right) dx \tag{4}$$

Alternatively, the error can be evaluated in the spectral domain. We rewrite the measured signal by defining two ISRF. The distorted ISRF can then be calculated:

$$\mathrm{L}_{measured}\left(\lambda_0, \lambda\right) = \mathrm{L}_0\left(\lambda_0\right) ISRF_{homo}\left(\lambda - \lambda_0\right) + \Delta\mathrm{L}\left(\lambda_0\right) ISRF_{hetero}\left(\lambda - \lambda_0\right) \tag{5}$$

$$ISRF_{distorted}\left(\lambda - \lambda_0\right) = \frac{\mathrm{L}_0\left(\lambda_0\right) ISRF_{homo}\left(\lambda - \lambda_0\right) + \Delta\mathrm{L}\left(\lambda_0\right) ISRF_{hetero}\left(\lambda - \lambda_0\right)}{\mathrm{L}_0\left(\lambda_0\right) + W\Delta\mathrm{L}\left(\lambda_0\right)} \tag{6}$$

Both radiometric and ISRF errors have been calculated for one of the two CarbonSat instrument concepts at end of phase A, assuming contrast scene #1 in ALT (Fig.1). The results are displayed on Fig.2 and Fig.3. We see that the radiometric error fluctuates around zero, consistent with a zero spectral average and a description in terms of ISRF distortion. The two contributors to the spectrally variable ISRF are plotted, as well as their relative weight. At first sight, the radiometric and spectral error descriptions seem to carry contradicting information: at the bottom of the absorption lines, the atmosphere becomes opaque and the weight of $ISRF_{hetero}$ is zero, giving no ISRF distortion while the radiometric error becomes maximum in this area, due to the presence of strong variations in the measurement. In the continuum where the ISRF distortion is the largest, the radiometric error is actually very small as the signal lacks spectral structure. In practice, the peak amplitude of

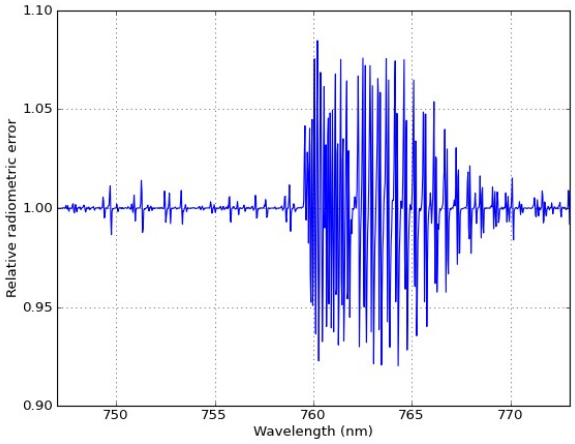

Fig. 2. Relative radiometric error created by contrast scene #1 in along-track, for one of the CarbonSat instrument concepts at end of phase A.

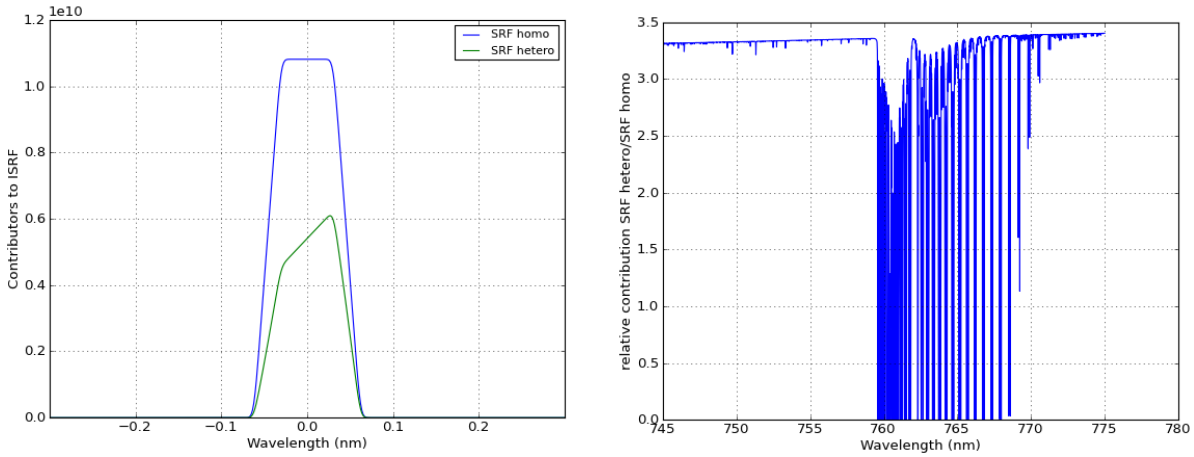

Fig. 3. Same error as in Fig.2 but described in the spectral domain. Components of the ISRF (left) and their relative weight (right). The integral of $ISRF_{hetero}$ is 0.5.

the radiometric error is quite sensitive to the exact shape of the lines in the measured spectrum and the assumed spectral grid, whereas the ISRF distortion remains stable and more suitable for performance assessment.

B. Slit homogenisers: principle and modelling

For Sentinel-5 and CarbonSat phases A-B1, a slit homogeniser (SH) device was considered to mitigate this error. In its standard form, it consists in a thick slit made of two highly reflective parallel mirrors separated by spacers (see Fig.4). The telescope (or spectrometer) must have some astigmatism: in the ACT direction, the telescope and spectrometer focal planes coincide to keep a perfect spatial image, while in the ALT direction, the telescope is focused at the SH entrance and the spectrometer at its exit.

Due to the narrow spectrometer bandwidth, a source point at the SH input must be considered as coherent so

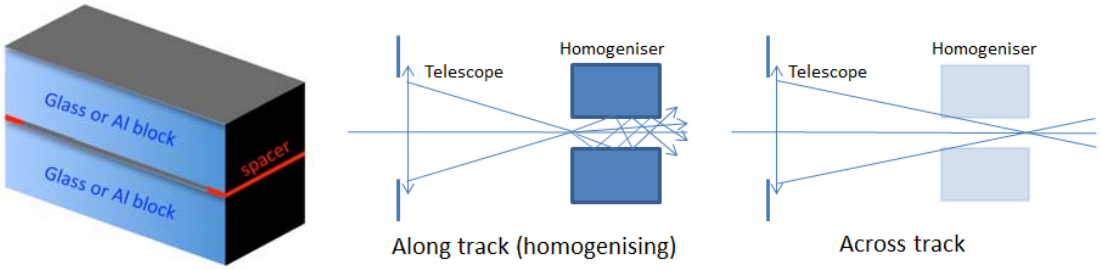

Fig. 4. Slit homogeniser device (left). The instrument must have some astigmatism: the telescope is focused at SH input in ALT (center) while in ACT the telescope and spectrometer focal planes coincide (right).

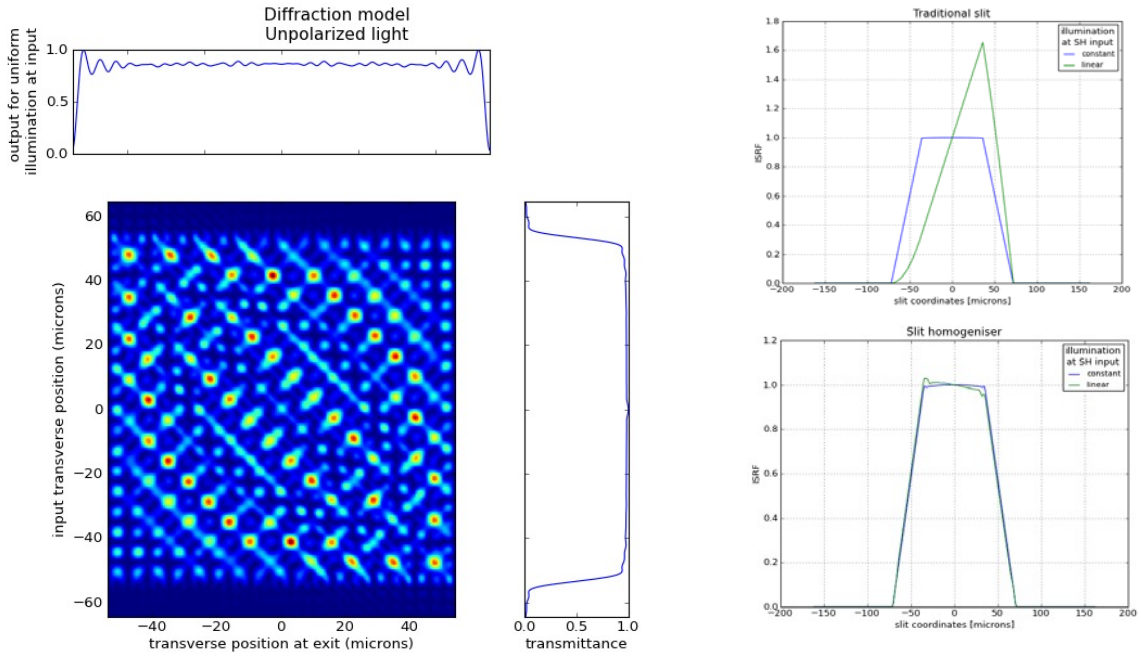

Fig. 5. Left: example of SH transfer function in NIR band with n~3. Right: ISRF obtained for uniform (equal to 1) and linear (from 0 to 2) illumination profiles, for a traditional slit (top) and the slit homogeniser (bottom).The ISRF intrinsic distortion values are respectively 65.7% and 3.78% with an improvement factor ~ 17 due to SH. Scrambler spot pattern, spectrometer aberrations and detector crosstalk are ignored.

that the superposition of all reflected beams at the SH exit creates an interference pattern. The slit homogeniser behavior is completely described by a so-called "transfer function", a 2D map giving the observed output interference patterns for each position of an input source point. An example of a transfer function is depicted on Fig.5. Summing the transfer function along one direction gives either the SH transmittance as a function of input stimulus position, or the output intensity profile for uniform illumination. Two possible approaches can be used for calculating transfer functions:

Geometrical optics model: the input stimulus is assumed to be a point emitting in a cone defined by the F number of the telescope optics. Propagation inside the slit homogeniser occurs along straight lines (rays). The length of each optical path is measured and the corresponding phase information is included when the complex intensities are summed up in the SH output plane. This model is simple but has the drawback to slightly violate energy conservation.

Diffraction model: the input stimulus is a diffraction PSF originating from the telescope. Mirror images of this diffraction PSF are computed to build a complex intensity profile over the complete SH input plane (not just the slit opening). Propagation to SH output is done with a diffraction integral. This model is a bit more complex but more accurate, it fulfills energy conservation and also describes the progressive decrease of transmittance when the diffraction PSF is moved towards the edge of the SH opening.

To improve the accuracy, the coating properties, with phase and amplitude may be easily inserted in the two above models. In most cases, a 1D model is sufficient as the optical path difference does not vary with the ACT pupil coordinate (this results from the perfect focusing required in the ACT to preserve the spatial image). The only difficulty comes for the case of a diffraction model with a circular pupil, where a 2D model is required. More elaborate models may be established to consider the impact of the scrambler pattern (the scrambler spots are mutually coherent, and may interfere if they have similar ACT coordinates and polarisation), the impact of the spectrometer pupil (it cuts the diffracted light at large angles, e.g. if the input PSF is close to the slit edges and partly clipped), and the impact of the spectrometer aberrations (the slit homogeniser strongly modifies pupil illumination in the spectrometer, altering the aberrations and then ISRF in a way that depends on SH input illumination).

C. Slit homogenisers: sizing and performance

To size the slit homogeniser, it is convenient to make simplifying assumptions on the instrument. With no polarisation scrambler and a diffraction limited telescope, the contrast scene #1 in ALT (Fig.1) is transformed with the satellite smear into a linear illumination at SH input, ranging from 0.5*(1-slit/smear_distance) at one

edge to 0.5*(1+slit/smear_distance) at the other. In that case the final ISRF distortion is given by a simple formula:

$$\delta ISRF\left(\lambda,\lambda_0\right)=\left(\frac{slit}{smear}\right)\left[\frac{L_{bright}\left(\lambda_0\right)-L_{dark}\left(\lambda_0\right)}{L_{bright}\left(\lambda_0\right)+L_{dark}\left(\lambda_0\right)}\right]\frac{ISRF_{linear}\left(\lambda,\lambda_0\right)-ISRF_{uniform}\left(\lambda,\lambda_0\right)}{\max_{\lambda}\left[ISRF_{uniform}\left(\lambda,\lambda_0\right)\right]} \quad (7)$$

The three terms in this equation provide the contributions from the slit width, the scene contrast and the SH intrinsic performance. $ISRF_{linear}$ is the ISRF obtained from a linear slope of illumination at SH input (varying from 0 at one edge to 2 at the other edge), and $ISRF_{uniform}$ is the ISRF obtained from a uniform illumination equal to 1. Both ISRFs are plotted on the right part of Fig.5.

As the slit width is generally determined from the radiometric and spatial resolution performances, sizing a slit homogeniser reduces to choosing its depth. For an instrument with a rectangular pupil it can be shown that depths with integer values of n = D/(2F#W) = 1,2,3... would give a perfect SH if there were no interferences (pure geometrical optics). In this equation F# is the relative aperture of the beam in the ALT direction, W the SH width and D the SH depth. In practice, these depth values still correspond to an optimal performance even accounting for the interferences. For a circular or elliptical pupil, the law is no longer valid but optimum performance can be achieved for typical values n>2.5.

For CarbonSat, the depth optimization was performed in all bands, and the final performance computed including all instrument contributions, in particular scrambler, spectrometer aberrations and detector crosstalk. The final ISRF distortion, over contrast scenes #1 and #2, fits in the budget of 1% accuracy for in-flight ISRF shape knowledge.

III. IMPACT OF ACROSS-TRACK SCENE HETEROGENEITIES

A. Effect of across-track heterogeneities with smile

If the slit image on the detector FPA is not exactly aligned with the spatial axis, the ISRF may be distorted due to ACT scene heterogeneities. This occurs in presence of spectrometer smile, but also if the detector has been slightly rotated. The error mechanism is described on Fig. 6: the slope of the slit image induces a shift in the ISRF barycenter if a spatial sample is partially illuminated [7]. As it directly impacts the ISRF, the error is a spectral one and has a similar radiometric signature as for non-uniform slit illumination in ALT (see Fig.2).

To simulate this error mechanism with the traditional PSF formalism, one has to separate artificially the imaging properties of the spectrometer (diffraction and aberrations) from the geometrical distortion (smile). This is in reality not possible as all these effects come from the same origin: optical wavefront distortion through the spectrometer. Nevertheless, one reasonnable possibility to describe spectrometer smile is to use a convolution with the Dirac function δ(x-Sy) where S is the local slope. For simplicity we also assume that the spectrometer-pixel PSF can be expressed as a product $PSF_1(x)PSF_2(y)$. The measured signal in presence of smile and ACT heterogeneities is given by an equation similar to (3):

$$\begin{aligned}L_{measured}\left(\lambda_0,\lambda\right)=&\left\{\left[L_0\left(\lambda_0\right)+\tilde{w}\left(y\right)\Delta L\left(\lambda_0\right)\right]Slit\left(x\right)\otimes\delta\left(x-Sy\right)\right\}\\&\otimes\left[PSF_1\left(x\right)PSF_2\left(y\right)\right]\otimes k\delta\left[x-k\left(\lambda-\lambda_0\right),y\right]\end{aligned} \quad (8)$$

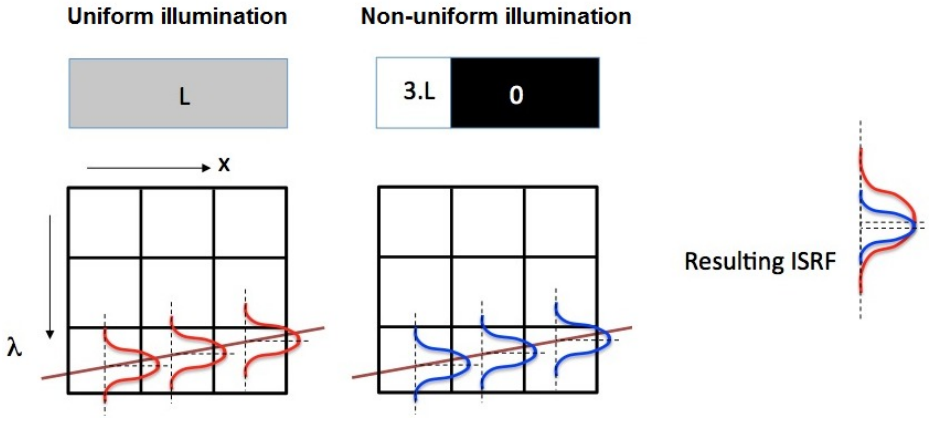

Fig. 6. Mechanism creating the ISRF distortion due to ACT non-uniform illumination and smile.

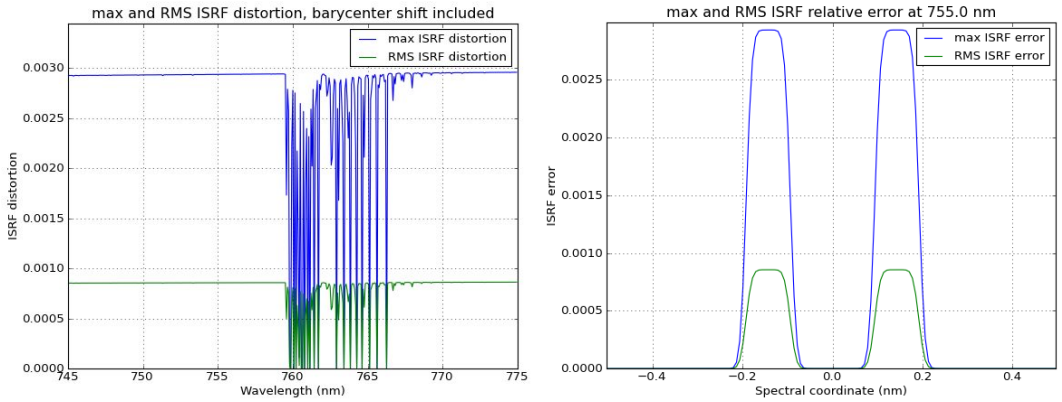

Fig. 7. Max and rms ISRF distortion, as a function of wavelength (left) and spectral coordinate (right).

In this formula, the order of the convolutions matters. Convolution with the smile Dirac function is performed in the first place (inside the brackets {}) so that all other convolutions are done with the transformed coordinates. This allows, for instance, to avoid a diffraction pattern distorted by the smile. The monochromatic measured signal can be then expressed as a weighted sum of $ISRF_{homo}$ and $ISRF_{hetero}$ as in (5). These two ISRFs can be expressed as a weighted superposition of shifted smile-free ISRFs, which is consistent with the description of Fig.6:

$$ISRF_{\substack{smile\\free}}(x) = Slit(x) \underset{x,y}{\otimes} PSF_{\substack{spectro\\detector}}(x,y) = Slit(x) \underset{x}{\otimes} PSF_1(x)$$

$$ISRF_{homo}(\lambda_0,\lambda) = \left[\int ISRF_{\substack{smile\\free}}(x - Sy')\, PSF_2(-y')\, dy'\right] \underset{x}{\otimes} k\delta\left[x - k(\lambda - \lambda_0)\right] \tag{9}$$

$$ISRF_{hetero}(\lambda_0,\lambda) = \left[\int ISRF_{\substack{smile\\free}}(x - Sy')\, \tilde{w}(y')\, PSF_2(-y')\, dy'\right] \underset{x}{\otimes} k\delta\left[x - k(\lambda - \lambda_0)\right]$$

The distorted ISRF is then calculated with an equation similar to (6), with W being replaced by W':

$$W' = \int \tilde{w}(y)\, PSF_2(-y)\, dy \tag{10}$$

The ISRF distortion was calculated over a few realistic scenes derived from AVIRIS data. The obtained figures vary proportionally with the assumed smile amplitude, so a reference local smile value of 10% of the spectral pixel over one spatial sample was used. The max and rms ISRF distortions obtained for one of the two CarbonSat concepts, over the city of Washington (AVIRIS dataset F090706t01p00r13, see Fig.1) are illustrated on Fig.7. The left plot, showing the ISRF distortion vs wavelength, is similar to what was obtained for ALT non-uniformities (Fig.3), with a maximum distortion occuring in the continuum. The right plot shows that the ISRF distortion occurs mostly at the ISRF edges, suggesting a strong contribution from a barycenter shift. The barycenter shift is zero at the bottom of the absorption lines due to the opaque atmosphere, leading to no distortion, and is maximum in the continuum.

B. Correction with spectral calibration and final performance

Unfortunately, even if accurately known, this barycenter shift cannot be corrected by spectral calibration in the NIR band, due to its too strong and fast spectral variability. To illustrate why, it is useful to introduce new concepts and clarify what is meant by ISRF. If λ is a incident monochromatic wavelength at the instrument's input, and λ_k the centroid of spectral channel k, the most general spectral response function $SRF(\lambda,\lambda_k)$ is mapping input wavelengths λ into measured wavelengths λ_k. This 2-dimensional function is shown, in presence of smile, on the left part of Fig.8. On this figure the impact of smile was purposely amplified by an order of magnitude to make the distortions easily visible. The ISRF, interpreted as the instrument response to a monochromatic stimulus, appears as a vertical slice of the SRF. Its integral is normalised to 1 due to energy conservation. The ISMF (Instrument Spectral Measured Response), which depicts the spectral origin of the measured photons in one spectral channel, is an horizontal slice of this response.

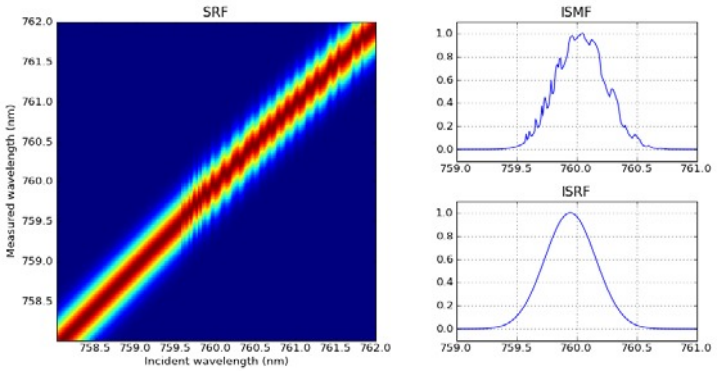

Fig. 8. SRF, ISRF and ISMF obtained with smile and ACT heterogeneities. The impact of smile has been purposely amplified for easier visualisation.

It is worth noting that on-ground calibration performed with a tunable laser actually provides the ISMF, not the ISRF. In general, if spectral properties have only slow variations, the ISRF and ISMF are mirror image of each other and the ISMF integral is also normalised to 1. Over ACT heterogeneous scenes and in presence of smile, this is no longer the case. We see on Fig.8 that the ISRFs are shifted vertically due to the impact of smile. This shift is highly variable and must be computed from the unconvolved spectra for each different monochromatic wavelength. The ISMF, that describes the spectral origin of each measured point and averages the scene contrast within a certain spectral interval, is unfortunately distorted so that the effect cannot be corrected by simple wavelength re-assignment.

Similar strongly variable shifts have been found in SWIR-2. For CarbonSat, smile values in the order of 10% (of the spectral pixel for one spatial sample) in NIR, 5% in SWIR-2 would create a rms ISRF distortion of 0.1%. The situation is dramatically different in SWIR-1 thanks to the shallow absorption bands and the resulting weak contrast variation. We found that the spectral shift in SWIR-1 is correctable to a large extent by spectral calibration, leaving no particularly demanding smile constraint.

IV. CONCLUSION

This paper describes the role of spatially heterogeneous scenes on the radiometric and spectral performances of CarbonSat. The cases of non-uniform slit illumination in ALT, and smile combined with ACT heterogeneities are studied in details with emphasis on the methodology description. The former is mitigated in CarbonSat with a slit homogeniser, whose principle and performance are described. The latter is tackled with dedicated requirements on spectrometer smile.

We acknowledge useful interactions with the contractors involved in the early phases of Sentinel-5 (Kayser-Threde gmbh, Airbus Defence and Space) and CarbonSat (Airbus Defense and Space, OHB/Thalès), as well as identification of the smile effect and communication to ESA by IUP Bremen [7].

REFERENCES

[1] R.Voors, M.Dobber, R.Dirksen, P.Levelt, “Method of calibration to correct for cloud-induced wavelength shifts in the Aura satellite's Ozone Monitoring Instrument”, Applied Optics, pp. 3652-3658, 2006.
[2] S.Noel et al., “Quantification and mitigation of the impact of scene inhomogeneity on Sentinel-4 UVN UV-VIS retrievals”, Atmos. Meas. Tech., 5, pp. 1319-1331, 2012.
[3] S.Noel, K.Bramstedt, P.Liebing, M.Vountas, H.Bovensmann, “In-flight spectral calibration and requirements on reflectance for Sentinel 4”, ESA Contract 4000101187/10/NL/MP/ef, Final report, 2011.
[4] S.Noel, K.Bramstedt, H.Bovensmann, “ Science support to instrument development for S4”, Final report, section5: Pseudo noise mitigation performance for S5, ESA Contract 4000104913/11/NL/MP/fk, v2, 2013.
[5] H.Bovensmann et al., “CarbonSat EE8 Candidate Mission: L2 and L1B Requirements Consolidation Study”, ESA Contract 4000105676/12/NL/AF, Final report (under review), 2014.
[6] J.L.Bézy et al., “The Copernicus Sentinel-5 mission for operational atmospheric monitoring: Status and Developments”, SPIE remote sensing 2014, in preparation.
[7] K. Gerilowski et al., MAMAP – a new spectrometer system for column-averaged methane and carbon dioxide observations from aircraft: instrument description and performance analysis, Atmos. Meas. Tech., 4, 215–243, 2011.